INVITED PAPER

Standoff Detection Using Millimeter and Submillimeter Wave Spectroscopy

Pollution and some traces of explosive materials can be detected in the upper atmosphere by these spectroscopy techniques; to improve existing capabilities, more sensitive receivers are needed.

By H. J. Hansen, *Member IEEE*

ABSTRACT | The millimeter (MM) wave and sub-MM wave (30–600 GHz) frequency band contains fundamental rotational and vibrational resonances of many molecular gases composed of carbon, nitrogen, oxygen, and sulphur. The high specificity of rotational spectra to organic molecules affords MM wave spectroscopy having potential use in remotely sensing atmospheric pollutants and the detection of airborne chemicals is important for arms control treaty verification, intelligence collection, and environmental monitoring. This paper considers the sensitivity requirements of radiofrequency receiver systems for measuring MM wave absorption/emission signatures. The significance of receiver sensitivity and material optical depth to sensing is highlighted. A background to the technology needed for sensing at MM and sub-MM wavelengths then provides the basis for a review of MM wave spectroscopy and its role on profiling the concentrations of trace polar molecules and ionized radicals in the high altitude atmosphere. The application of the MM wave spectroscopic technique in ambient conditions is then reviewed and the issues associated with developing the technique for standoff remote sensing is discussed.

KEYWORDS | Millimeter wave; remote sensing; spectroscopy; trace detection

Manuscript received September 30, 2005; revised March 23, 2007. This work was supported in part by the RF HUB of the Australian Defence Science and Technology Organisation (DSTO).

The author is with Electronic Warfare and Radar Division, Defence Science and Technology Organisation, Edinburgh, SA 5111, Australia (e-mail: hedley.hansen@dsto.defence.gov.au).

Digital Object Identifier: 10.1109/JPROC.2007.900331

I. INTRODUCTION

The millimeter (MM) wave region of the electromagnetic spectrum, occupying the frequency range from 30 to 600 GHz (8–0.5 mm wavelength), lies between the micro (μ) wave and infrared (IR) wave regions [1]. The sub-MM wave region is also considered as the lower part of the terahertz (T) wave region.

MM wave spectroscopy utilizes the unique specific absorption and emission spectral lines of chemical structures in order to identify materials [2]–[4]. At μ and MM wave frequencies exist the fundamental rotational resonances for diatomic molecules composed of carbon, nitrogen, and sulphur, and therefore spectral line measurements associated with these resonances are invaluable for atmospheric ozone studies and for understanding the chemistry of outer space [2], [3].

In contrast with outer space and upper atmospheric regions, the exploitation of MM wave spectroscopy in the terrestrial environment has proved unattractive. This relates partly to the natural radiation spectrum of most gaseous materials being dominated by transitions between vibrational states that give rise to emissions in the higher IR region of the electromagnetic spectrum. In addition, those lower energy rotational states that tend to give rise to MM and μ waves typically have low radiation levels and the emissions are broadened due to the collision-dominated molecular interactions that occur at atmospheric temperatures and pressures [2], [4].

Operating radiometric sensors at smaller wavelengths (towards the T-ray band) show that pressure broadening effects can be overcome because the broader bandwidths, typical of higher frequency sensors, improve spectral line resolution and hence molecular selectivity [5]–[7]. While this is encouraging for possible sub-MM

wave interrogation of sites for toxic and trace pollutants [2], how this methodology would complement other more established trace detection methods (e.g., dog sniffing, x-ray screening, neutron scattering, nuclear quadrupole resonance) is unclear [8], [9].

Remote sensing using MM waves has always been attractive, particularly to the military. There is a strong interaction of these waves with airborne molecules associated with chemical and nuclear proliferation facilities [2], and MM waves suffer far less attenuation in the atmosphere in the presence of water vapor, smoke, fog, and dust compared to optical and IR waves [10], [11]. With the push for T-ray systems for a wide range of medical and security monitoring applications, there has been renewed activity in MM wave sensing [12]. The emergence of high radiofrequency (RF) components, fabricated with gallium arsenide (GaAs) and indium phosphide (InP)-based monolithic microwave integrated circuit (MMIC) technologies [13], are able to provide the tens of gigabyte samples/second and broadband signal handling capability for real-time remote sensing applications using MM wave and sub-MM wave radiation. Modern radiometers are capable of detecting 0.01 K signals [3], [10], [11], and as these levels improve, spectral methods will be increasingly exploited in atmospheric constituent studies.

This paper considers the development of remote chemical detection systems for defense-related trace detection and surveillance applications. The structure of the paper is as follows. The next section provides a tutorial outlining spectroscopic principles and associated absorption measurement processes. The importance of receiver sensitivity to sensing is then demonstrated by considering the radiative transfer process in a simple remote sensing scenario [7]. Measured optical depths enable projected performance assessments of state-of-the-art receiving systems to be performed. A review of MM wave spectroscopy as a diagnostic tool in upper atmosphere constituent studies is provided. Finally the issues associated with developing sub-MM detection systems for security-type trace-explosive detection applications are discussed.

II. SPECTROSCOPIC PRINCIPLES AND ABSORPTION AND EMISSION PROCESSES

Molecular spectroscopy is based on the permanent intrinsic dipole moment of a molecule interacting with an oscillatory electric field component of radiation causing a transition between the molecule's rotational states. Suppose a gas molecule is able to change from energy state E_u to E_l emitting radiation of frequency

$$\nu_{\mathrm{lu}} = \frac{E_u - E_l}{h}. \tag{1}$$

Einstein showed between any two energy levels either: i) spontaneous emission with probability $p_{\mathrm{ul}} = UB_{\mathrm{ul}} + A_{\mathrm{ul}}$ (the subscripts indicate transition from higher energy level u to lower energy state l); ii) absorption with probability $p_{\mathrm{lu}} = B_{\mathrm{lu}}U$ (where U is the average density of the radiation field); or iii) simulated emission with probability $B_{\mathrm{ul}}U$ is possible.

From time-dependent perturbation theory

$$p_{\mathrm{lu}} = \frac{8\pi^3}{3h^2}\left[\langle l|\mu|u\rangle\right]^2 \rho(\nu_u) \tag{2}$$

where $\langle l|\mu|u\rangle = \int \psi^* \mu \psi d\tau$ is the dipole moment expectation value and so

$$B_{\mathrm{lu}} = \frac{8\pi^3}{3h^2}\langle l|\mu|u\rangle^2 \tag{3}$$

where $\langle l|\mu|u\rangle$ are the matrix elements of the dipole moment components resolved on the space-fixed axis in the representation which diagonalizes the energy matrix of the molecule [4], [14].

The coefficients A_{ul}, B_{lu}, and B_{ul} are dependent according to

$$B_{\mathrm{lu}} = \left(\frac{g_2}{g_1}\right) B_{\mathrm{ul}} \tag{4}$$

where g_i is the degeneracy of the ith state and

$$A_{\mathrm{ul}} = \left(\frac{8\pi h \upsilon^3}{c^3}\right) B_{\mathrm{ul}} \tag{5}$$

where h is Planck's constant, ν is the frequency, and c is the speed of light.

These dependencies are linked to the radiation field following Planck's distribution, and to the molecules occupying available states in accordance with the Boltzmann distribution [4], [14].

The absorption coefficient α in the Beer Lambert (BL) law expression is the macroscopic quantity associated with quantum mechanical spectral line processes. Fig. 1 depicts the absorption of radiation by gas molecules as radiation passes through cell ydx. The lowered intensity is written $\Delta I = -\alpha I dx$ and so the BL law, $I = I_o e^{-\alpha x}$ (where α is the absorption coefficient) follows, where I equates to the average energy density times the speed of light, viz., $I = Uc$.

The link between α and the Einstein absorption coefficient can be demonstrated from previous approaches

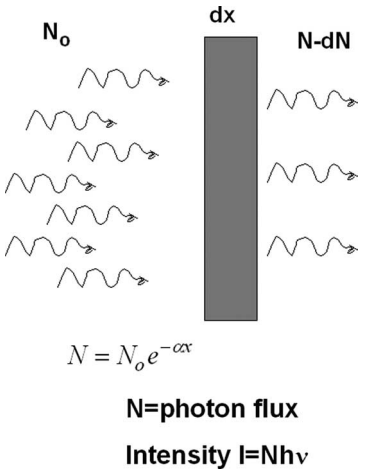

Fig. 1. ***Absorption as radiation passes through medium of path length*** *dx*.

([4], [14]) and this is now outlined. Because thermal motion keeps the population N of states l and u different, viz., $N_u = N_l e^{(-h\nu_{lu})/kT}$, perturbation theory allows the energy absorbed $\Delta E = (N_l - N_u,)h\nu_{lu}$ associated with the number of molecules involved in going from state l to u, to be formulated as

$$\Delta E = N_l\left[1 - e^{\frac{-h\nu_{lu}}{kT}}\right]h\nu_{lu}. \tag{6}$$

Expressing this number of molecules ΔN quantum mechanically, the particle density (per unit volume) $\Delta N/V \equiv B_{lu}U\Delta N$ becomes the appropriate quantity, and in unit time, the associated energy (or power ΔP) absorbed

$$\Delta P = -\left\{VB_{lu}UN_l(1 - e^{-h\nu/kT})h\nu_{lu}\right\} \tag{7}$$

provides the BL exponential decay form $\Delta P = -\alpha P dx$. According to Fig. 1 volume cell $V = Ydx$ and energy flow $P = UYc$ (where c is the speed of light), and so substituting for V and U in (7) leads to a

$$\alpha_{lu} = \frac{N_l}{c}\left[1 - e^{-\frac{h\nu_{lu}}{kT}}\right]B_{lu}h\nu_{lu} \tag{8}$$

absorption coefficient term for the lu transition.

The transitions between l and u states are the same for all molecules present in a Boltzmann distribution. The Heisenberg Uncertainty Principle explains the association of a natural band (or line) width with the frequency measurement of any spectral line and both Doppler and pressure broadening effects are also present. Consequently there is a need to multiply (8) with a normalized shape function for it to be useful in the terrestrial environment. At low pressures (≤ 1 mm Hg), the Lorentzian line-shape function, viz., $S(\nu_{lu}, \nu) = (1/\pi)[\Delta\varphi/((\nu_{lu} - \nu)^2 + (\Delta\varphi)^2)]$ is used, where the integrated absorption peak occurs at ν_o and $\Delta\varphi$ is the half-width of line between half-intensity points. At higher pressures > 10 mm Hg, the more general Van Vleck–Weisskopf expression

$$S(\nu_{lu}, \nu) = \frac{\nu}{\pi\nu_o}\left[\frac{\Delta\nu}{(\nu_{lu} - \nu)^2 + (\Delta\nu)^2} + \frac{\Delta\nu}{(\nu_{lu} + \nu)^2 + (\Delta\nu)^2}\right]$$

is appropriate. Consequently, (8) becomes

$$\alpha_{lu} = \frac{N_l}{c}\left[1 - e^{-\frac{h\nu_{lu}}{kT}}\right]B_{lu}h\nu_{lu}S(\nu_{lu}, \nu). \tag{9}$$

Since α_{lu} exhibits a maximum value when frequency $\nu = \nu_{lu}$, it is useful to express (8) as

$$\alpha_{lu} = \alpha_{lu(max)}\frac{(\Delta\varphi)}{(\nu_{lu} - \nu)^2 + (\Delta\varphi)^2}. \tag{10}$$

The total absorption coefficient over a band of frequencies requires accounting for those spectral transitions occurring at other frequencies ν_i in the band, i.e.,

$$\alpha_{total} = \sum_i \alpha_{imax}\frac{(\Delta\varphi)^2}{(\nu_i - \nu)^2 - (\Delta\varphi)^2} \tag{11}$$

which is the starting expression for most applied spectroscopic studies [2], [4], [14].

Radiative transfer theory, describing the passage of radiation through absorbing material, refers to the material's emissivity ε and opacity α values. These quantities allow the material to be regarded as a blackbody. The change in intensity I is expressed as

$$\frac{dI}{dx} = -\alpha_\nu I_\nu + \varepsilon_\upsilon \tag{12}$$

where dx is the slab thickness, dI is the change in intensity, α_ν is the opacity, and ε_ν is the emissivity [3]. If there is complete equilibrium of the radiation with its surroundings, $dI/dx = 0$ and the brightness distribution is described by Planck's energy density function, which depends only on the thermodynamic temperature T of the

surroundings. A more general equation of transfer also involving spontaneous emission (Einstein coefficient A) becomes

$$\frac{dI}{dx} = -\frac{h\nu}{c}(N_l B_{\mathrm{lu}} - N_u B_{\mathrm{ul}}) I_\nu \varphi(\nu) + \frac{h\nu}{4\pi} N_u A_{\mathrm{ul}} S(\nu) \quad (13)$$

where N_l denotes the occupancy of the ith state, I_ν the intensity, and $\mathsf{S}(\mathsf{v})$ the line profile [3].

From inspection of (12) and (13), the opacity α_ν or absorption coefficient is given by

$$\alpha_\upsilon = -\frac{h\nu}{c}(N_l B_{\mathrm{lu}} - N_u B_{\mathrm{ul}}) \quad (14)$$

which because of (5) becomes

$$\alpha_\nu = \frac{c^2}{8\pi}\frac{1}{\upsilon}\frac{g_2}{g_1} A_{\mathrm{ul}} \left[1 - \exp\left(-\frac{h\upsilon}{kT}\right)\right] S(\nu) \quad (15)$$

where k is Boltzmann's constant and T is the temperature. Significantly, this links the macroscopic absorption coefficient with the radiation rate associated with a particular spectral line profile. In the literature, Einstein coefficients A_{ij} are used to calculate opacity values, which are compared with opacities obtained from absorption measurements [3], [5], [6].

III. METHODOLOGY

A. Passive Detection

Passive RF sensing involves the detection of naturally occurring electromagnetic radiation with radiometers. Radiometers are widely used in radio astronomy and atmospheric sensing applications in which sensor measurements are obtained using antennas (located on land on aircraft) pointing towards the upper atmosphere or outer space. The detectability of absorbing material is determined by the receiver's sensitivity. This is demonstrated by adopting the approach given in [7].

Fig. 2 considers a cloud of gas pollutant of brightness B_c and thickness D embedded in background of brightness B_g. A radiometer, sensing from an aerial platform, receives emissions from the cloud and also a contribution from the atmosphere B_a. The total brightness associated with the radiation detected has been expressed as

$$B_T = B_c e^{-\tau_c} + (B_g - B_c) e^{-(\tau_a + \tau_c)} + B_a \quad (16)$$

where τ_c is the optical thickness of the cloud, and τ_a is the optical thickness of the atmosphere between the sensor

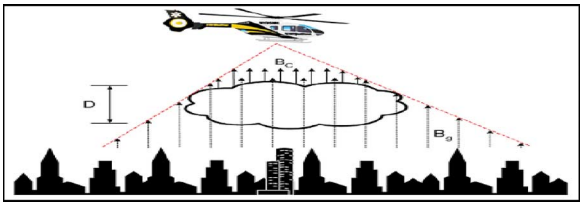

Fig. 2. *A passive airborne radiometer receives radiation from chemical cloud of thickness D according to BL Law.*

and the cloud [7]. The optical thickness τ is defined to be $\tau = \alpha D$ where, as before, α is the absorption coefficient (in Np per unit length). At radio frequencies Planck's Law allows brightness to be written as

$$B = \frac{2kT}{\lambda^2} \quad (17)$$

where λ is the wavelength and so (16) becomes

$$T_T = T_c e^{-\tau_c} + (\varepsilon_g T_g - T_c) e^{-(\tau_a + \tau_c)} + T_a \quad (18)$$

where for backgrounds of emissivity ε_g, $B_g = \varepsilon_g T_g$. Typically τ_a is a minor term, therefore (18) approximates to

$$T_T = T_c(1 - e^{-\tau_c}) + \varepsilon_g T_g e^{-\tau_c} + T_a. \quad (19)$$

When the pollutant cloud is not present, $T_T = \varepsilon_g T_g + T_a$. Consequently, the observable signal associated difference between these T_T values is

$$\Delta T_{\mathrm{obs}} = (T_c - \varepsilon_g T_g)(1 - e^{-\tau_c}) \approx (T_c - \varepsilon_g T_g)\tau_c. \quad (20)$$

The detection system must be sensitive to ΔT_{obs} signal levels. However because the sensitivity of a radiometric receiver is given by

$$\Delta T_s = \frac{T_{\mathrm{system}}}{\sqrt{B\tau}} \quad (21)$$

the observed signal-to-noise ratio is

$$\mathrm{SNR} = \frac{\Delta T_{\mathrm{obs}}}{\Delta T_s}. \quad (22)$$

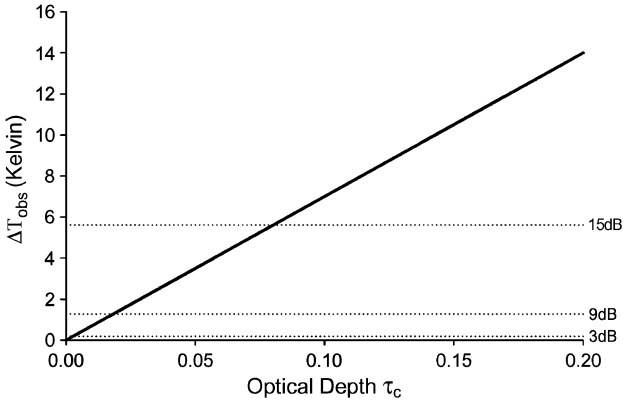

Fig. 3. *The receiver sensitivity and absorbing medium's optical depth variation.*

Equations (20) and (22) relate the detectability of spectral absorption lines (in terms of the optical thickness parameter) to the noise performance of a receiver. A measured signal exhibits a power level above the detecting system's noise level and this is affected by the background $(T_c - \varepsilon_g T_g)$ [7]. For a typical air-to-ground scene ($T_g = T_c = 80$ K, $T_c = 80$ K, $\varepsilon_g = 0.5$), Fig. 3 shows the variation in observed signal level with absorbing medium (optical depth). Assuming SNRs $= 1$, the signal level values relate to receiver sensitivity (ΔT_s), which determines the material (τ) it can detect. The dotted lines indicate the sensitivities of typical (noise $= 3$, 9, and 15 dB) receivers, assuming bandwidth $B = 500$ MHz and sampling period $\tau = 5$ ms. The $\Delta T_s = 0.18$ K temperature difference is associated with a 3 dB noise level, a value typically exhibited by state-of-the-art cryogenic radiometric systems for astronomical-grade measurement [3]. The $\Delta T_s = 5$ K value corresponds to a 15 dB noise value, which is typical of sensitivities exhibited by receiver architectures designed for radiometric electronic support measure (ESM) applications.

B. Active Detection

Active remote sensors process electromagnetic transmissions with tuned receiver systems. Fig. 4 depicts a bistatic arrangement where the receiver and transmitter are displaced from each other. The received signal is given by the radar equation

$$P_{\mathrm{Ro}} = \frac{P_T G_T A_R}{4\pi R^2} \tag{23}$$

where the terms have their usual meaning. For radar emissions propagating through an absorbing medium of optical thickness τ, the attenuated signal received becomes

$$P_R = P_{\mathrm{Ro}} e^{-\tau}. \tag{24}$$

Active sensors measure a signal change given by

$$S_{\mathrm{obs}} = P_{\mathrm{Ro}}(1 - e^{-\tau}) \tag{25}$$

with an associated signal-to-noise ratio of

$$\frac{S}{N} = \frac{S_{\mathrm{obs}}}{\Delta T_s} \tag{26}$$

where ΔT_s is given by (21).

MM wave spectroscopy researchers [5]–[7] provided normalised absorbance measurements given by

$$A = \log_{10}\left(\frac{S_{\mathrm{obs}}}{P_{\mathrm{Ro}}}\right) = \log_{10}(1 - e^{-\tau}) = 0.43\tau \tag{27}$$

where the optical depth τ is expressed in Nepers (Np). Optical depth in dB is related to optical depth in Nepers by

$$\tau_{\mathrm{dB}} = 10\frac{\tau_{\mathrm{Np}}}{\ln(10)} = 4.342\tau_{\mathrm{Np}}[5]. \tag{28}$$

Active sensing is more sensitive than passive detection because coherent sources operate at signal levels far above background levels.

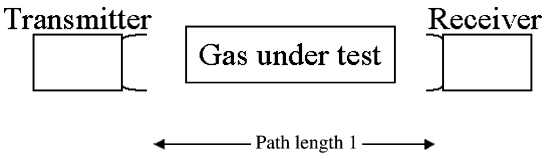

Fig. 4. *An active bistatic transmitter-receiver experiment.*

IV. MILLIMETER AND SUBMILLIMETER WAVE RECEIVERS

The MM and sub-MM wavelengths present great challenges to receiver engineers. At radio frequencies thermal noise processes (i.e., kT) determine the sensitivities of sensors. At IR and optical wavelengths, quantum effects (i.e., $h\upsilon$) are significant. At sub-MM wavelengths, neither thermal effects nor quantum effects are negligible and both must be considered.

At the heart of every RF receiver is a local oscillator and mixer. During the 1970s the local oscillator was a reflex klystron, phase-locked to a harmonic of a reference signal. This achieved the frequency stability necessary for spectral line measurements. The first receivers used room temperature components and consisted of a waveguide mounted Schottky diode used as a heterodyne mixer. Since the conversion loss of this mixer was substantial (~6 dB) it was necessary to follow this component with the lowest noise intermediate frequency (IF) amplifier available. Consequently the low noise amplifier (LNA) has played the most significant role in determining the noise performance of RF sensors.

The heterodyne architecture still dominates radio receiver design. Gunn oscillators, as the source of local oscillator power, have since replaced the short-lived klystron oscillators. Over the last couple of decades noise reduction has been achieved through improved diode fabrication, due to better understanding of the noise mechanism in Schottky barrier devices and through adopting cryogenic cooling of the mixer and IF amplifier front-end [16].

Since the 1980s, solid-state device RF receiver design for operation at MM wavelengths, up to 60 GHz, has relied on GaAs based MMIC device technology. Above 60 GHz, solid-state RF components depend on semiconductor bandgap and heterojunction engineering [17]. Operating at MM wave frequencies is still beyond the capability of CMOS based silicon devices and therefore the digital cell phone revolution has not impacted on MM and sub-MM wave sensing. The slow pace in the development of improved MM wave technology does relate to the demand for sensors primarily being driven by the astronomical and remote sensing research community. Consequently the RF front-ends emerging are experimental demonstrators that are custom made and expensive. At 100 GHz, the single-sideband noise temperature of the best available receivers in 1970 was ~2000 K [16]. Today this noise temperature is < 20 K. A state-of-the-art MM wave receiver for astronomical applications (at ~110 GHz) would most likely involve a cryogenically cooled LNA, where the LNA would involve InP high electron mobility transistor (HEMT) MMICs [17], [18].

GaAs technology has also been instrumental in the development of electrooptic integration. Electrooptic receivers could facilitate the handling of several octaves of bandwidth necessary for molecular fingerprinting in ambient conditions [2]. GaAs provides a direct bandgap which has been exploited in optical applications as detectors and light sources [19], [20]. The direct bandgap enables the interfacing of GaAs devices to the high speed digital and fiber optic link technologies. The use of optical signal transport is common in astronomy and necessary within receivers operating above 200 GHz. This is because the loss in fundamental mode waveguide increases with frequency and because the fabrication of sub-MM sized waveguide is very difficult. It has been reported that the monolithic integration of an optoelectronic modulator with a heterojunction bipolar transistor (HBT) driver circuit on an InP substrate achieved 30 GHz bandwidth with no degradation of the HBT by the modulator circuit fabrication procedures [21].

During the 1980s, astronomical spectroscopy has developed for radiation above 100 GHz through the maturity of superconductor–insulator–superconductor (SIS) tunnel junction semiconductor devices. The SIS junction has a nonlinear tunneling conductance associated with an energy gap of a few millielectron volts. SIS based devices appear capable of exhibiting gain and having sensitivity close to the quantum limit [16]. A SIS mixer, formed by planar lithography, is rugged and fabricated such that extra circuit elements for matching are easily provided along the junction. A further significant advantage of the SIS mixer is that the local oscillator power requirements are approximately 30 dB lower than that required for powering the typical Schottky mixer. This is proving compelling in high-frequency operations where mW sources are at a premium. Receiver noise temperatures of < 100 K at 115 GHz and ~150 K at 230 GHz have been reported with SIS devices using waveguide mixer mounts.

V. MILLIMETER AND SUBMILLIMETER WAVE REMOTE SENSING IN THE INTER STELLAR AND UPPER ATMOSPHERE ENVIRONMENTS

The development of MM wave spectroscopy is closely linked to spectral line radio astronomy and interstellar chemistry. Radio observations of atomic hydrogen emitting at a wavelength of 21 cm were first used in the 1960s to provide pictures of clouds of atomic hydrogen with densities of 10 to 50 atoms cm^{-3} and of temperatures 50 K–125 K spanning the intergalactic medium. The subsequent OH radical emission at a wavelength of 18 cm and the emission associated with formaldehyde (H_2CO) studies were not only significant in gaining an understanding of the complexity of the chemistry of intergalactic space but unearthed MM wave band spectral measurements as the diagnostic for probing the constituents of space [22]. The fundamental rotational transition frequencies for the diatomic molecules, composed of atoms C, N, O, and S lie in the range of 50 to 150 GHz, and the lowest frequency rotational transitions are typically 10 to 50 GHz for simple polyatomic molecules. For example, CO, the most abundant molecule within the Milky Way galaxy, emits at 115 GHz [21]. Fig. 5 indicates the information available from MM and sub-MM observations of interstellar clouds [16]. It shows a complex spectrum for which a plethora of heavy molecules are indicated. Fig. 5 also reveals the difficulty of identifying spectral signatures in ambient terrestrial conditions. The low-frequency transitions of

CO usually reflect the gas temperature and these are indicated as reaching the black body curve. For high values of the rotational quantum number, CO molecules tend to become subthermally excited and emit less strongly, so the line densities drop below the 30 K black body curve. In ambient conditions, CO molecules occupy excited states.

At MM wavelengths, the atmospheric absorption characteristic shows troughs, corresponding to transmission bands and peaks, corresponding to absorption bands. The transmission bands cover 24 to 48 GHz, with attenuation values between 0.1 and 0.3 dB km^{-1}; 70 to 110 GHz, with attenuation values between 0.3 and 1 dB km^{-1}; 120 to 155 GHz, with attenuation values between 1 and 2.5 dB km^{-1} and 190 to 300 GHz, with attenuation values between 2 and 10 dB km^{-1}. Of the large number of atmospheric gases that have resonances in the MM wave part of the spectrum only oxygen and water vapor have significant absorption characteristics. The sea level absorption data, shown in Fig. 6 [24], are clearly not a line spectrum, but a spectral continuum that results from the broadening of oxygen and water vapor lines by pressure and temperature dependent molecular collisions. The 50 to 70 GHz frequency band contains 43 oxygen absorption lines. A single oxygen line also exists at 118.75 GHz. Water vapor has electric dipole moments at about 22 GHz, 183 GHz and a further 150 resonant lines distributed throughout the sub-MM wave part of the spectrum. For surface conditions (i.e., ≈760 Torr and $T \approx 300$ °K) the continuum spectrum applies. At altitudes above 20 km, the line spectrum applies.

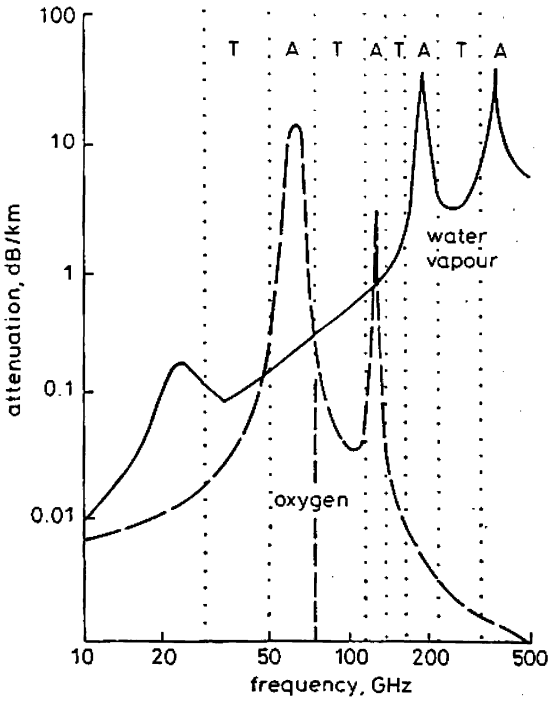

Fig. 6. *The mm-wave attenuation due to oxygen and water vapor after [22]).*

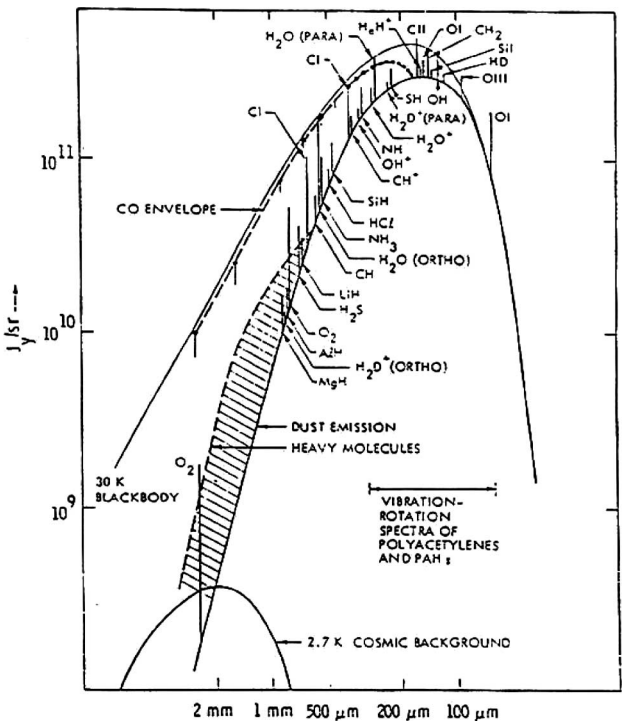

Fig. 5. *The mm-wave spectral content in interstellar clouds (after [22]).*

Passive μ-MM wave radiometry is a highly developed method for monitoring the morphology and dynamics of the Earth's atmosphere. Meteorological forecasting relies on oxygen and water vapor spectral line measurements, and the detection of trace pollutants relies on the unique resonances exhibited by different molecules in the 100 to 800 GHz band. With global warming and ozone depletion being major concerns, MM wave investigations, under the auspices of the numerous North American and European space and environmental agencies (e.g., Canadian Space Agency, Environment Canada, European Space Agency, Jet Propulsion Laboratory, National Aeronautical and Space Administration, Swedish Space Corporation) are widespread. The studies outlined below are not exhaustive but do provide an indication of the importance of MM and sub-MM wave measurements to investigating atmospheric processes.

Radiometer measurements recorded on spacecraft, aircraft, balloon, and the ground are used for atmospheric constituent profiling and surface feature sensing in meteorology. Spacecraft observations are capable of monitoring the entire atmosphere at regular intervals. Oxygen spectral line measurements, at 60 and 118 GHz, are used for vertical temperature profiling [24]. Those associated with water vapor, e.g., at 183 GHz, are used for

vertical water vapor content profiling. Parameters, such as these, are derived as follows. At a resonance, the radiative emission detected by a satellite borne radiometer is from the top of the atmosphere, whereas at frequencies on the side of the resonance, the radiative emission comes from lower altitudes. Therefore correlating any resonant signal with appropriate weighting coefficients (derived from calibration measurements and knowledge of the atmosphere) yields the parameter (temperature or water content) relevant to the resonance. Sounders, operating at 60 GHz, were flown on TIROS-N weather satellites and paved the way for the development of an Advanced Microwave Sounding Unit (AMSU) that has been flown on NOAA satellites. AMSU has 20 channels covering MM waves in the 20 to 200 GHz range in two parts. As examples of ground-based MM wave systems used in weather studies, NOAA operates portable two channel (23.87 and 31.35 GHz) and three channel (20.6, 31.65, and 90 GHz) radiometers for detecting thermal emissions by liquid water and water vapor. These provide information about the spatial and temporal variability of liquid water in clouds and atmospheric water vapor.

Radiometers are used for all-weather mapping and for obtaining images of the sea and ice. These systems are mounted below aircraft and use raster scanning to build up pictures of swathes of land or sea as the aircraft travels along. Atmospheric windows at about 33, 90, 140, and 220 GHz have been used to determine the ice thickness and the location of the sea-ice edge, and to differentiate ice types in the polar regions. For example, Finnish investigators have used multifrequency measurements to classify different sea-ice types in the Baltic Sea [25]. The sea surface has been observed from both aircraft and satellites to determine how the structure of surface waves depends on factors such as wind speed, e.g., SEASAT carried a 37 GHz radiometer. W-band emissions (90 GHz) have measured snow cover area and in a slightly different application, radiometers at 35 and 90 GHz have been used to measure the thickness and quantity of oil on water [26]. The European Space Agency (ESA) has developed the multifrequency imaging microwave radiometer (MIMR) that comprises six dual-polarization frequency channels in the 7 to 92 GHz range. This radiometer images emissions from the earth's surface using the six frequency bands and so makes measurements that are used for weather monitoring, climate change, and resource management applications (snow, ice, and forestry) [27], [28].

In the area of remote sensing of trace gases, MM wave systems are important in monitoring ozone (O_3) levels in the middle atmosphere because a number of ozone's rotational transition lines occur at MM wave frequencies. MM wave spectral measurements (e. g., 142 GHz) provide the only means of monitoring the ozone chemical depletion process in the mid-altitude (from 10 to 100 km) atmosphere. It has been established that the decrease in ozone content is due to the photo-disassociation of freons, released by aerosols and other human activities. Every ozone destruction process produces a chlorine oxide (ClO) radical, a compound with a characteristic spectral line at 204 GHz that is widely studied. Radiometers, operating from satellite and aircraft platforms, are favored over ground-based measurements in ozone studies because the pressure broadening spectral line width effect of the lower atmosphere can be avoided. The effect is minimized by adopting a horizontal (as opposed to vertical) viewing experimental geometry and consequently, the measurements from horizontal viewing radiometer systems, termed limb sounders, are currently providing the most detailed information about the ozone depletion process. Examples of aircraft related investigations are found within the framework of the European Arctic Stratospheric Ozone Experiment (EASOE). Heterodyne receivers on high flying German FALCON aircraft (9 to 12 km altitude) have operated around the ClO, HCl, and N_2O emission lines in the 625 to 655 GHz range [29]. A new receiver using an SIS waveguide mixer [termed airborne sub-MM radiometer (ASUR)] has been developed that measures in the 626 to 760 GHz band of frequencies [30]. Nevertheless, most information is coming from limb sounders, operating from satellites, because satellites provide greater daily coverage and reach a larger range of altitudes than do aircraft. Important MM wave and sub-MM wave limb sounders exist on the Upper Atmosphere Research Satellite [UARS—the Halogen Occulation Experiment (HALOE)], the space shuttle (the MM wave atmospheric sounder—MAS) and on the Odin spacecraft (the sub-MM wave radiometer—SMR). MAS measures radiation at 61, 62, 63, 183, 184, and 204 GHz and provides profiles for oxygen, water vapor, ozone, and chlorine monoxide at 10 to 100 km altitudes. The Odin radiometer package (118 to 119 GHz; 486 to 504 GHz; 541 to 580 GHz) covers the spectral line transitions of ClO, CO, NO_2, N_2O, H_2O_2, HO_2, H_2O, $H_2{}^{18}O$, NO, HNO_3, O_3, and O_2 molecules, gases which are of aeronautical (mid-altitude 15 to 120 km) interest. Widespread ground-based experiments are augmenting these spacecraft studies. For example, measurements of the 142 GHz rotational line of O_3 have been used within the European Stratospheric Monitoring Stations (EMOS) network to provide ozone profiles on a global scale [31]. The German and Swedish MIllimeter wave RAdiometry (MIRA) team operates a 268 to 279 GHz experiment at Kiruna and Svalbard that provides vertical profiles of stratospheric CIO, O_3, HNO_3, and N_2O at these sites [32]. Other concurrent ground-based and spacecraft observations, e.g., water vapor measurements recorded with the ground-based Water Vapor MM wave Spectrometer (WVMS) network, and H_2O, CH_4, and NO_2 measurements from HALOE, have provided important information about water vapor's role in controlling the free radicals responsible for ozone depletion [33].

VI. MILLIMETER AND SUBMILLIMETER WAVE SENSING IN THE TROPOSPHERE

Pressure broadening of rotational transition spectral lines critically diminishes their intensity and capability to signature the presence of trace chemicals in air at atmospheric pressure. At atmospheric pressures, these linewidths are 5 GHz. Closer analysis reveals the challenges in achieving remote sensing capability in the troposphere are orders of magnitude more difficult than in the upper atmosphere and in outer space.

Firstly, the atmosphere's transmission characteristic shows there are < 100 5 GHz transmission windows and this hinders the information channels available for the specific detection of gaseous molecules.

Secondly, unlike in harsh nonambient environments, it is very difficult to separate the MM wave spectral line features of a particular analyte from the sensor system fluctuations and from background noise [34]. In ambient environments the background noise (or atmospheric clutter) relating to the temporal fluctuations of broadened spectral lines can overwhelm weak spectral line signatures [11], [12].

Despite these problems there has been progress in standoff remote sensing. Sensitivity is proportional to frequency squared and better sensitivity at higher frequencies of operation helps offset the low intensities of the transitions. In addition measurements above 200 GHz, provided in particular by BWOs sweeping over wide bandwidths (> 100 GHz), have achieved partial mitigation of the spectral linewidth broadening effect [35]–[37]. Broadband MM wave spectrometers, operating in the 215 to 315 GHz frequency range have been built at the Argonne National Laboratory [5]. The BWO tubes (Model OB-30 from Istok Corporation, Russia) used delivered an average power of 10 mW and allowed the entire 225–315 GHz range to be swept in 10 ms. Concentrations of ~12 ppm methyl chloride were detected at 60 m standoff distances. Fig. 7 shows the setup and detection measurements associated with 150 ppm concentrations of methyl chloride [37]. The phase locked control of the BWO was too slow for the wide-frequency sweep required in open-path spectroscopy and so a quasi-optical Fabry–Pérot cavity for on-the-fly calibration of frequencies was used.

The idea of remote sensing chemical warfare (CW) materials has emerged from the U.S. Army Edgewood Chemical and Biological Center [2] in which they describe the Fourier transform μ wave spectroscopic (FTMWS) extractive gas technique, for specifying the rotational spectral lines of chemical structures in order to identify and quantify chemical materials. Even though low-pressure investigations are unsuited to standoff (remote sensing) operations, they demonstrated that applying the FTMS technique does allow for the CW agent μ wave spectra to be catalogued. Knowledge of the lowest energy rotational transitions enables the determination of the associated higher harmonic frequency spectral transitions and it is at higher frequencies (above 100 GHz), where pressure broadening is mitigated [2]. FTMW measurements on two nerve agents, Sarin (methyl-phosphono-flouridic acid (1-methyl-ethyl) ester(GB),CAS# 107-44-8) and Soman (Methyl-phosphono-flouridic acid, 1,2,2-trimethyl-propyl ester (GD), CAS# 96-64-0), and of the vesicant agent H-Mustard (1,1′-Thio-bis{2-chloro-ethane(H), CAS# 505-60-2), were studied. Fig. 8 shows the rotational spectrum for Sarin, and Fig. 9 shows the predicted broadened spectra that would "fingerprint" Sarin and Soman in ambient conditions.

There has been further effort in developing extractive gas methods that utilize the rotational signatures of molecules for diagnosing gas phase polar molecules. In IR and UV spectroscopy, rotational signatures appear as unresolved bands at MM and sub-MM wave frequencies; however, closer detail shows the bands exhibit Doppler limited linewidths typically ~1 MHz. Since the analysis of gaseous samples at pressures (~1 mTorr) reduces the pressure broadened linewidths to Doppler limit widths and separates the spectral lines, the fast sub-MM-wave terahertz technique (FASST) has emerged which, in essence, emulates the upper atmospheric region in a gas cell, and relies on using BWOs to scan 100 GHz in a fast enough time (3 s) to yield 10^5 Doppler resolution elements [34]. The technique is dependent on employing bright radiation sources of high purity (BWO) and relies on large amounts of computing power. Fig. 10 shows a solid-state system with spectral details associated with a mixture of four gases (concentrations ~1 ppm). Because atmospheric clutter (oxygen water vapor and pollutants) appears to concentrate its power in negligibly few of the Doppler resolution elements [34], the technique does exhibit potential as a diagnostic for analyzing point samples of tropospheric gases. As the availability of high-frequency solid-state detectors and sources and computing power improves (in response to the demand from the wireless communications and collision avoidance sectors) emerging systems should become low-cost in the future. It is, however, not a standoff remote sensing technique but a sampling method that can be bracketed with the trace detection methods (which include the neutron, nuclear quadrupole resonance (NQR) ion mobility spectrometry, and dog sniffing) discussed in the next section.

Currently, there is much interest in the development of T-radiation sources. Thermionic devices (e.g., high powered traveling wave tubes, gyrotrons) are the traditional sources for signals up to W-band (75–120 GHz) and kW levels of power have been provided for military and satellite-communication applications [24]. Solid-state radiation sources deliver much smaller levels of power at MM wave and higher sub MM wave frequencies. A survey of the techniques available for generating sub-MM/T-radiation reveals that the current state-of-the-art optically pumped terahertz laser (OPTL) would be the only

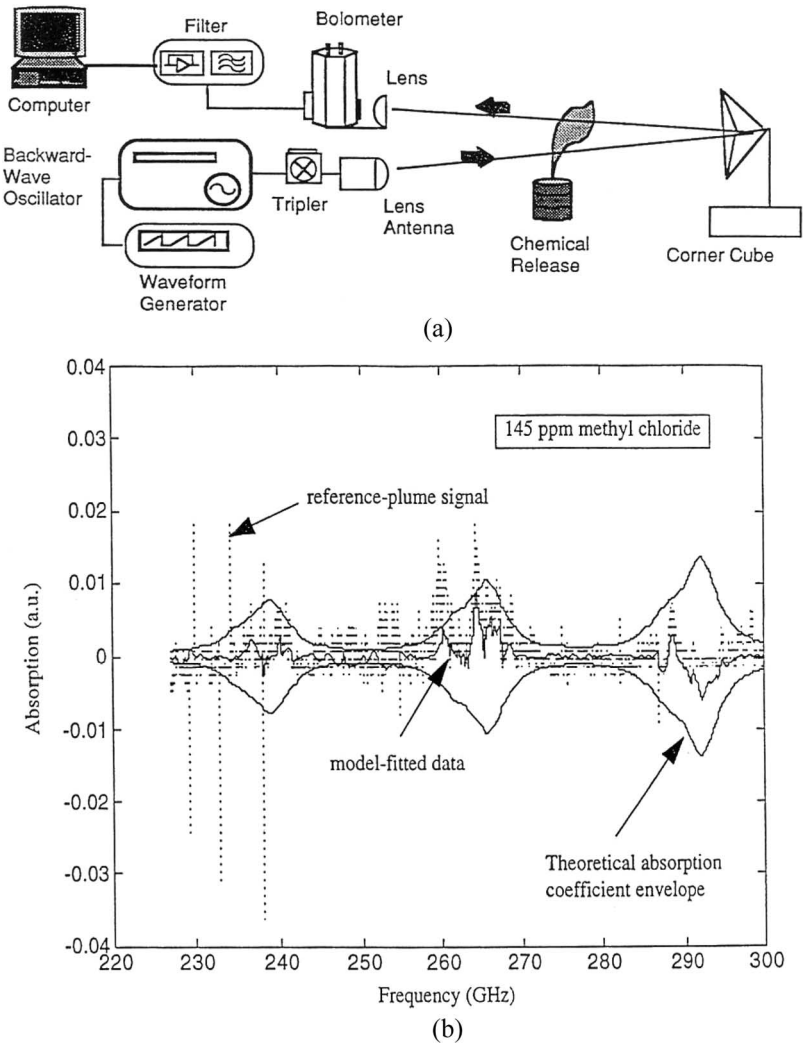

Fig. 7. *(Above) Experimental 215–315 GHz spectrometer in open path measurement sit-up (after [5]). (Below) Absorption of trace methyl chloride in ambient conditions. The difference signal between the reference and the plume (the dotted line), model-fitted signal (the solid line) and the absorption coefficient envelope (solid line) is shown (after [6]).*

available continuous wave source capable of generating workable levels of power (100 mW) for environmental monitoring and astronomy at frequencies < 300 GHz. Below 500 GHz, BWOs and multiplied-up RF oscillators do provide turnkey systems but the power sources are inefficient and the levels are low (< 10 mW). The small signal levels delivered by the many source technologies are of concern for ambient environment operation because atmospheric clutter overwhelms weak spectral signatures.

It has been suggested that the time-domain spectroscopy methodology (TDS) associated with current short-pulsed low power ($\sim\mu$W) T-ray sources might circumvent the atmospheric clutter problem because low duty cycles are expected to yield low background noise signals. In TDS, image construction relies on selective absorption causing delays in arrival time at the detector [38]–[40]. Fig. 11 shows a TDS set-up for medical imaging [38]. The sample-under-test is a tooth and therefore the image shown relates to phonon-mode waves in solids, rather than the rotational and vibrational gaseous modes of concern in this paper. Because the TDS measurement principle also applies to gaseous samples, recent studies suggest that until pulsed T-wave sources are closer to the continuous wave sources in brightness, the continuous wave approach will outperform the pulsed wave method in atmospheric-based diagnostics [34], [41], [42].

VII. DISCUSSION AND CONCLUSION

Detection sensitivity of an instrument depends on the noise level of the receiver and on the absorption strength

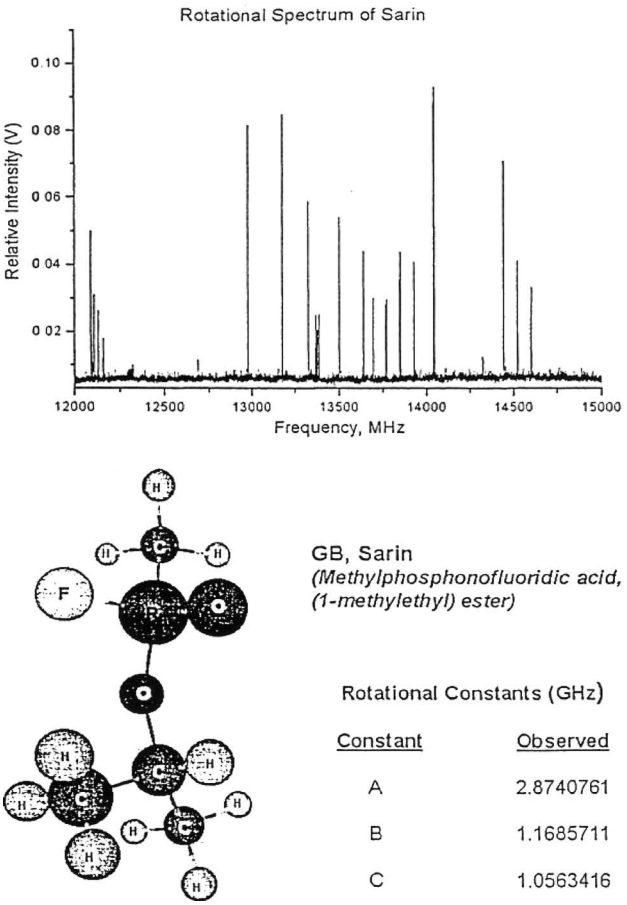

Fig. 8. *(Above) Rotational spectrum of Sarin with (below) Sarin's structure and rotational constants (after [2]).*

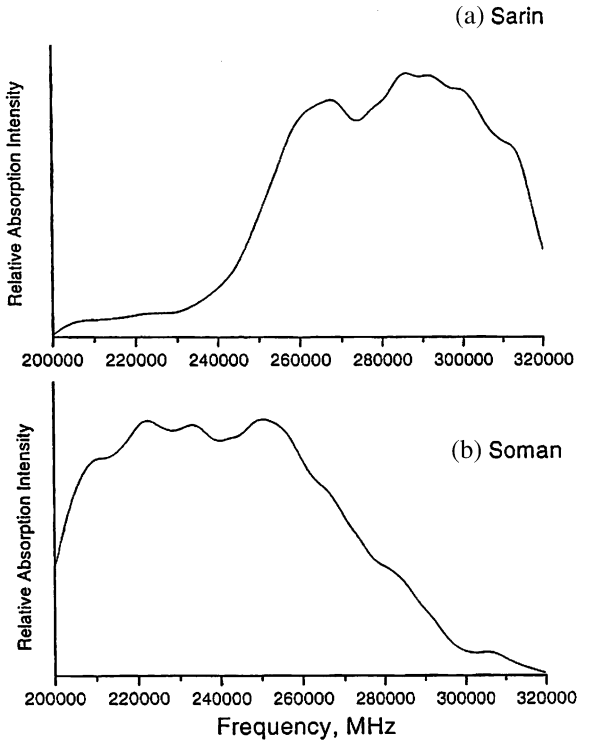

Predicted broadened spectra at high frequency using experimental Sarin and Soman parameters. Linewidth set at 5GHz for the purpose of the simulation.

Fig. 9. *Predicted spectra for Sarin and Soman under ambient conditions (after [2]).*

of the spectral peak associated with the molecule being detected. Ammonia, CH_3Cl, and H_2S (the molecules that have been considered in proof-of-concept studies) [5]–[7], [43], [44] are high dipole moment molecules that exhibit spectral transitions at higher frequencies that are much stronger than atmospheric clutter. The general applicability of the FASST and TDS methodologies to other than special molecules has yet to be demonstrated.

Future work should concentrate on developing receiver front-ends sensitive enough for passive measurement, on identifying the spectral features of atmospheric pollutants associated with rocket and other exhaust fuels and active studies in open air should be extended to higher frequencies in the sub-MM wave region of the electromagnetic spectrum [5]–[7]. At room temperatures, the natural frequencies of most molecules lie in the IR and therefore receiver development above 100 GHz is necessary. Ozone mid-latitude observations and a plethora of other atmospheric constituent gas studies (e.g., NO_2, CO, CH_3CL, etc.) are based on spectral line measurements above 100 GHz [5]–[7], [45], and a recent report suggests

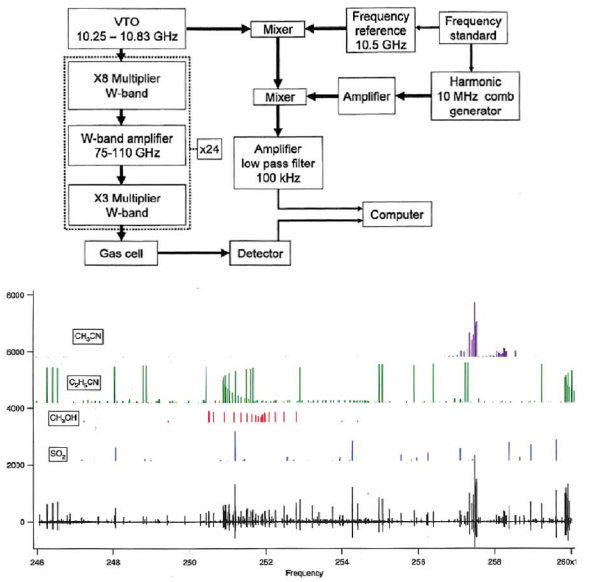

Fig. 10. *(Above) A solid-state implimentaton of the FASST technique. (Below) Spectra of four a gas mixture for which partial pressures were ~2 mmTorr (after [34]).*

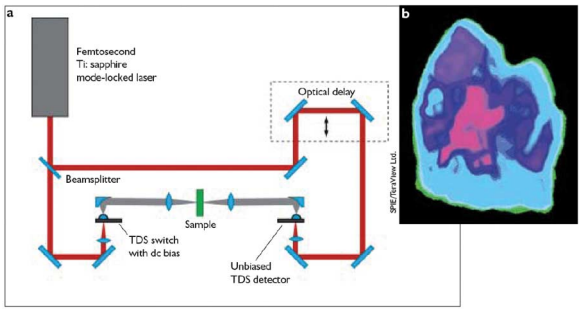

Fig. 11. *TDS yielding a tomography of a decayed tooth (after [38]).*

that the 600 GHz band [8], [12], [46] might be useful for covert anthrax detection in civilian security applications. The outlook for sub-MM spectroscopy techniques is encouraging because at higher frequencies sensitivity improves [5] and the rapid sweeping bandwidth systems that are emerging [5]–[7], [34] are capable of mitigating against the spectral linewidth broadening exhibited by measurements recorded in ambient conditions.

Much of the gas pollutant and explosive material of interest to homeland security agencies exhibit characteristic spectral lines throughout the sub-MM wave bands [8], [12]. While it is realized that some of these reports relate to wave-material coupling mechanisms different from the vibrational and rotational modes associated with gaseous vapors (e.g., phonon modes in solids, and particle absorption of powdered substances) there is value in comparing the concentrations of absorbing species in different experiments. This is because the BL law, expressing measured absorbance as a function of concentration of absorbing species (via the absorption coefficient), is generic to many physical and chemical processes. From the diagnostic perspective of standoff remote sensing in the atmosphere, the concentration of absorbing material in the presence of other atmospheric absorbers relates to the relevance of gaseous phase detection, an issue separate from the microscopic details of the absorption process.

Fig. 12 plots the concentration of explosive materials in air, evaluated from the ratio of their partial vapor pressures with that of air (at 298 K). Ammonia and hydrogen sulphide (H_2S) are also included. The high vapor pressure group, which includes ethylene glycol dinitrate (EGDN), nitroglycerine (NG), and dinitro toluene (DNT), exhibits part-per-million (ppm) concentrations in air. The medium vapor pressure group, which includes trinitrotoluene (TNT) and ammonia nitrate, is associated with the part-per-billion (ppb 10^{-9}) range of concentrations. Finally, the low vapor pressure group exhibits saturated concentrations in air in the part-per-trillion (10^{-12}) range. It has been suggested that the projected detection limits are in general 100 ppm, e.g., hydrogen sulfide has a spectral line at 305 GHz that has been resolved (spectral peak = 3.8%) in open-air experiments and using a partial pressure = 1.5 torr, a detection limit $D = \sim$120 ppm was evaluated [5]. This material is therefore important as a frame of reference for ascertaining the suitability of MM wave spectroscopy for gaseous diagnostics. An improvement in signal-to-noise ratio values exhibited by existing sensors is required (i.e., spectral peaks of < 0.23 % need to be resolved) to enable sub-MM wave spectroscopy to detect the medium and low vapor pressure materials indicated in Fig. 12.

Although this projection of detection sensitivity for explosives requires confirmation because prior knowledge of spectral frequencies and linewidths is needed, existing evidence suggests it is likely. First, the overall polarizations of large molecules are less than those of light ones and therefore the dipole moments of heavy explosive molecules cannot be expected to be larger than those of those molecules (e.g., NH_3, CH_3Cl, and H_2S) diagnosed. With this in mind, it is reasonable to expect that the detection challenges presented by the atmospheric clutter environment will remain an issue irrespective of the spectral details of any explosive. Second, Fig. 12 relates detection sensitivity to molecular size and a factor in past literature focusing exclusively of light molecule detection is that only light molecule diagnosis has been within the technological capabilities of radio and radar detection systems.

Finally, a comment on the relationship between sub-MM wave spectroscopic method and those other techniques used in trace explosive detection. These techniques have been divided into bulk and trace detection methods [8], [9], [12]. In general, the bulk methods, which include x-ray screening and MM wave imaging, are suitable for

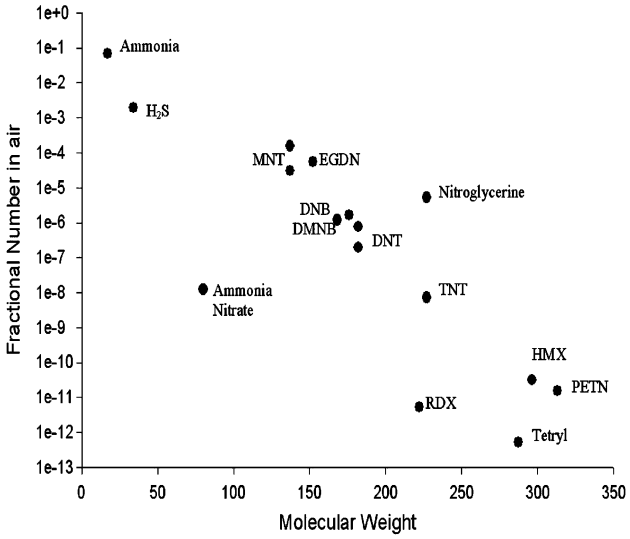

Fig. 12. *The vapor concentrations of explosive material in air.*

archway and passenger screening scenarios. On the other hand, the trace detection techniques provide detailed chemical and structural analysis of suspect objects. These include neutron, nuclear quadrupole resonance (NQR), ion mobility spectrometry, and dog sniffing. These techniques are able to detect parts-per-billion to fraction of parts-per-trillion (in the case of dogs) concentration levels, but the downsides to them include requiring typically tens of second sample and processing times, their lack of simplicity in operation and direct (particulate) or gaseous sampling. Sub-MM wave spectroscopy could be developed to complement the existing methods used to detect high vapor pressure materials such as EDGN and NG (e.g., such as ion mobility spectrometers or electron capture detectors) [8], [9], [12]. Although the sub-MM wave spectroscopic method offers potential standoff capability because of readily available coherent sources of power at < 500 GHz frequencies, it would appear that any gas phase method would at best complement the existing methodologies used for detecting medium and low vapor substances. The medium vapor pressure materials currently test the limits of gas phase detection methods, and the detection of low vapor pressure materials (concentrations ~ppb and ppt) is beyond the capability of the techniques described in this paper. ■

Acknowledgment

The support of the DSTO Hub is gratefully acknowledged.

REFERENCES

[1] R. G. Reeves, A. Anson, and D. Landen, Eds., *Manual of Remote Sensing*, 1st ed. Falls Church, VA: Amer. Soc. Photogrammetry, 1975, vol. 1.

[2] A. C. Samuels, J. O. Jensen, R. D. Suenram, A. H. Walker, and D. Woolard, "Microwave spectroscopy of chemical warfare agents: Prospects for remote sensing," *Proc. SPIE Passive Millimeter-Wave Imaging Technology III, 7 April 1999*, vol. 3703, pp. 121–129, 1999.

[3] K. Rohlfs and T. L. Wilson, *Tools of Radio Astronomy*. New York: Springer-Verlag, 1999.

[4] W. Gordy and R. L. Cook, *Microwave Molecular Spectra*. New York: Wiley, 1984.

[5] N. Gopalsami, S. Bakhtiari, A. Raptis, S. L. Dieckman, and F. C. Delucia, "Millimeter wave measurements of molecular spectra with application to environmental monitoring," *IEEE Instrum. Meas. Mag.*, vol. 45, no. 1, pp. 225–230, Feb. 1996.

[6] N. Gopalsami and A. C. Raptis, "Millimeter wave sensing of airborne chemicals," *IEEE Trans. Microw. Theory Tech.*, vol. 49, no. 4, pt. 1, pp. 646–653, Apr. 2001.

[7] N. Gopalsami and A. C. Raptis, "Millimeter-wave imaging of thermal and chemical signatures," *Proc. SPIE Passive Millimeter-Wave Imaging Technology III, 7 April 1999*, vol. 3703, pp. 130–138, 1999.

[8] M. C. Kemp, P. F. Taday, B. E. Cole, J. A. Cuff, A. J. Fitzgerald, and W. R. Tribe, "Security applications in terahetz technology," *Proc. SPIE*, vol. 5070, pp. 44–52, 2003.

[9] C. L. Rhykerd, D. W. Hannum, D. W. Murray, and J. E. Parmeter, *Guide for the Selection of Commercial Explosives Detection Systems for Law Enforcement Applications: NIJ Guide 100-99*, U.S. Justice Department, NCJ 178913, 1999. [Online]. Available: http://www.ncjrs.gov/pdffiles1/nij/178913.pdf

[10] D. G. Gleed, A. H. Lettington, R. Appleby, S. Price, N. A. Salmon, R. N. Anderton, G. N. Sinclair, and J. R. Borrill, "Operational issues for passive millimeter wave imaging systems," *Proc. SPIE Passive Millimeter-Wave Imaging Technology*, vol. 3064, pp. 23–33, 1997.

[11] C. Martin, J. Lovberg, S. Clark, and J. Galliano, "Real time passive millimeter-wave imaging from a helicopter platform," *Proc. SPIE Passive Millimeter-Wave Imaging Technology IV*, vol. 4032, pp. 22–28, 2000.

[12] J. Xu, H. Lui, T. Yuan, R. Kersting, and X.-C. Chang, "Advancing terahertz time-domain spectroscopy for remote detection and tracing," *Proc SPIE*, vol. 5070, pp. 17–26, 2003.

[13] M. G. Case, C. Pobanz, S. Weinreb, M. Matloubian, M. Hu, M. Wetzel, P. Janke, and C. Ngo, "Low-cost, high-performance W-band LNA MMICs for millimeter-wave imaging," *Proc. SPIE Passive Millimeter-Wave Imaging Technology IV*, vol. 4032, pp. 89–96, 2000.

[14] C. H. Townes and A. L. Schawlow, *Microwave Spectroscopy*. New York: Dover, 1955.

[15] G. L. Hey-Shipton and A. W. Denning, "Millimeter-wave block converters," *Tech-Notes*, vol. 16, no. 6, Nov./Dec. 1989. [Online]. Available: http://www.wj.com/documents/Tech_Notes_Archived/Scanned_Tech_Notes/vol_16_n6nov_dec89.pdf

[16] J. M. Payne, "Millimeter and submillimeter wavelength radioastronomy," *Proc. IEEE*, vol. 77, no. 7, pp. 993–1014, Jul. 1989.

[17] S. Weinreb, "Noise temperature estimates for next generation very large microwave array," in *IEEE MTT-S Int. Microwave Symp. Dig.*, 1998, vol. 2, pp. 673–676.

[18] J. Archer, M. W. Sinclair, A. Daddello, S. Giugni, R. G. Gough, G. Hincelin, S. Mahon, P. Roberts, O. Sevimli, and X. Wang, "Millimeter wave integrated circuits for radio astronomy and telecommunications," in *Proc. Workshop Applications of Radio Science 2000*, pp. 198–203.

[19] G. Zhao, R. N. Schouten, N. van der Valk, and W. T. Wenckebach, "Design and performance of a THz emission and detection setup based on a semi-insulating GaAs emitter," *Rev. Sci. Instrum.*, vol. 47, pp. 1715–1719, 2002.

[20] B. Ferguson and X.-C. Chang, "Materials for terahertz science and technology," *Nature Mater.*, vol. 1, pp. 26–33, 2002.

[21] D. Yap, K. R. Elliot, Y. K. Brown, A. R. Kost, and E. S. Ponti, "High-speed integrated optoelectronic modulation circuit," *IEEE Photon. Technol. Lett.*, vol. 13, no. 6, pp. 626–628, Jun. 2001.

[22] P. Solomon, "Interstellar molecules," *Phys. Today*, vol. 26, pp. 32–40, 1973.

[23] R. W. Wilson, K. B. Jefferts, and A. A. Penzias, "Carbon monoxide in the Orion nebula," *Astrophys. J.*, vol. 116, p. 44, 1970.

[24] A. D. Olver, "Microwave systems—Past present future," *IEE Proc.*, vol. 136, no. 1, pt. F, pp. 35–52, 1989.

[25] L. Kurkvonen and M. Hallikainen, "Airborne microwave radiometer measurements of Baltic sea ice," *Microwave Radiometry and Remote Sensing of the Environment*, D. Solimini, Ed. Utrecht, The Netherlands: VSP, 1995, pp. 347–356.

[26] N. Bartsch, K. Gruner, W. Kaydai, and F. Witte, "Contributions to oil spill detection and analysis with radar and microwave radiometry," *IEEE Trans. Geosci. Remote Sens. E*, vol. GE-25, no. 6, pp. 677–690, Nov. 1987.

[27] R. Bordi, M. L. Abbate, and P. Spera, "Multifrequency imaging microwave radiometer: Design, calibration and expected performance," in *Microwave Radiometry and Remote Sensing*, VSP Utrecht, D. Solimini, Ed., pp. 469–483, 1995.

[28] S. Contu, F. M. Marinelli, and P. Rinous, "Antenna electrical design for the multifrequency imaging microwave dadiometer: MIMR," *Microwave Radiometry and Remote Sensing of the Environment*, D. Solimini, Ed. Utrecht, The Netherlands: VSP, 1995, pp. 499–508.

[29] H. Nett, S. Crewell, and K. Kunzi, "Heterodyne detection of stratospheric trace gases at submillimeter-wave frequencies," in *Proc. 11th Annu. Int. Geoscience and Remote Sensing Symp.*, 1991, pp. 201–204.

[30] J. Mees, S. Cresswell, H. Nett, G. de Lange, H. van de Stadt, J. J. Kuipers, and R. A. Panhuyzen, "ASUR—An airborne SIS receiver for atmospheric measurements of trace gases at 625 to 760 GHz," *IEEE Trans. Microw. Theory Tech.*, vol. 43, no. 11, pp. 2543–2548, Nov. 1995.

[31] W. C. Zommerfelds, K. F. Kunzi, F. E. Summers, R. M. Bevilaqua, D. F. Strobel, M. Allen, and W. J. Sawchuck, "Diurnal variations of mesospheric ozone obtained by ground-based microwave radiometry," *J. Geophys. Res.*, vol. D10, pp. 12 819–12 832, 1989, 94.

[32] G. Hochschild, H. Berg, G. Kopp, R. Krupa, and M. Kuntz, "Profiles of stratospheric ClO and O_3 simultaneously retrieved from millimeter wave radiometry at Ny-Alesund (Svalbard) during March 1997," in *Proc. IEEE Int. Geoscience and Remote Sensing Symp.*, 1998, pp. 2618–2620.

[33] G. E. Nedoluha, R. M. Bevilacqua, R. M. Gomez, B. C. Hicks, and J. M. Russell, III, "Measurements of middle atmospheric water vapour from low latitudes and midlatitudes in the northern hemisphere," *J. Geophys. Res.*, vol. 104, pp. 19 257–19 266, 1999.

[34] F. C. De Lucia and D. T. Petkie, "THz gas sensing with sub-millimeter techniques," in *Proc. SPIE Terahertz for Military and Security Applications*, 2005, vol. 5790, pp. 44–53.

[35] J. Bredow, A. K. Fung, D. P. Gibbs, and S. Tjuatja, "A 75–110 GHz millimeter-wave spectrometer for pollution studies," in *Proc. IEEE Int. Geoscience and Remote Sensing Symp.*, 1994, pp. 693–695.

[36] A. Nadimi and J. Bredow, "Preliminary evaluation of a millimeter-wave system for air pollution monitoring," *IEEE Proc.*, pp. 863–865, 1996.

[37] N. Gopalsami and A. C. Raptis, "Remote sensing of chemicals by millimeter wave spectroscopy," *Proc. SPIE*, vol. 3465, pp. 254–265, 1998.

[38] E. R. Mueller, "Terahertz radiation: Application and sources," *Ind. Phys.*, vol. 9, no. 4, pp. 27–33, 2003.

[39] D. M. Mittleman, R. H. Jacobsen, R. Neelamani, R. G. Barunik, and M. C. Nuss, "Gas sensing with terahertz time-domain spectroscopy," *Appl. Phys.*, vol. B67, pp. 379–384, 1998.

[40] S. A. Harmon and R. A. Cheville, "Parts-er-million gas detection from long baseline THz spectroscopy," *Appl. Phys. Lett.*, vol. 85, pp. 2128–2130, 2004.

[41] F. C. De Lucia, "Spectroscopy in the terahertz spectral region," in *Sensing With Terahertz Radiation*, D. Mittleman, Ed. Berlin, Germany: Springer, 2003, pp. 39–116.

[42] F. De Lucia, "Noise detectors and submmillimeter-terahetrz performance in non-ambient environments," *J. Opt. Soc. Amer.*, vol. B 21, pp. 1273–1297, 2004.

[43] H. Harde, J. Zhao, M. Wolff, R. A. Cheville, and D. R. Grischkowsky, "THz time-domain spectroscopy on ammonia," *J. Phys. Chem.*, vol. A105, pp. 6038–6047, 2001.

[44] M. Szlazak, S. Y. Yam, D. Majstorovic, H. Hansen, and D. Abbott, "Remote gas detection using Mm-wave spectroscopy for counter bio-terrorism," *Proc. SPIE*, vol. 4937, pp. 73–83, 2002.

[45] N. A. Salmon and R. Appleby, "Carbon monoxide detection using passive and active millimeter wave radiometry," *Proc. SPIE Passive Millimeter-Wave Imaging Technology IV*, vol. 4032, pp. 119–122, 2000.

[46] E. R. Brown, D. L. Woolard, A. C. Samuels, T. Globus, and B. Gelmont, "Remote detection of bioparticles in the THz region," in *Proc. 2002 IEEE Int. Microwave Symp.*, 2002, vol. 3, pp. 1591–1594.

ABOUT THE AUTHOR

H. J. Hansen (Member, IEEE) was born in Port Elizabeth, South Africa, in 1957. He received the B.Sc. (Hons), M.Sc. (*cum laude*), and Ph.D. degrees from the University of Natal, Durban, South Aftrica, in 1980, 1983, and 1988, respectively. His Ph.D. research was concerned with magnetospheric wave particle interaction processes that give rise to the optical aurora.

In 1988, he joined the Space Plasma Waves Group at the University of Newcastle, NSW, as a Postdoctoral Research Associate. The group maintained arrays of induction magnetometers in Australian Antarctic Territory and across the Australian Mainland. He moved to RF Technology Group, Electronic Warfare and Radar Division, Defence Science and Technology Organisation, Edinburg, South Australia, in 1996 as a Senior Research Scientist. His professional interests lie in RF remote sensing at millimeter and submillimeter wavelengths, in microstrip antenna design, and in phased array and miniaturized radar technologies.

Dr. Hansen currently chairs the AP&MTT Chapter (South Australian section) of the IEEE. He is member of both the American Geophysical Union (AGU) and the Australian Institute of Physics (AIP).